Hydrometeorological Processes and Moisture Sources in the Northeastern Tibetan Plateau: Insights from a 7-Yr Study on Precipitation Isotopes🖉

HUAWU WU,[a,b] CICHENG ZHANG,[c] XIAO-YAN LI,[b] CONGSHENG FU,[a] HAOHAO WU,[a] PEI WANG,[b] AND JINZHAO LIU[d]

[a] Key Laboratory of Watershed Geographic Sciences, Nanjing Institute of Geography and Limnology, Chinese Academy of Sciences, Nanjing, China
[b] State Key Laboratory of Earth Surface Processes and Resource Ecology, Beijing Normal University, Beijing, China
[c] College of Resources and Environmental Science, Hunan Normal University, Changsha, China
[d] State Key Laboratory of Loess and Quaternary Geology, Institute of Earth Environment, Chinese Academy of Sciences, Xi'an, China

ABSTRACT: The northeastern Tibetan Plateau is located in a climatic junction, which is considered an ideal region to explore the interactions between the summer monsoons and the westerly circulation patterns. However, to date, the needed long-term precipitation-based isotopic dataset is too limited to predict the interactions and patterns. This paper presents an evaluation of hydrometeorological processes and climate dynamics in the northeastern Tibetan Plateau based on a 7-yr precipitation isotope dataset covering the summer monsoon periods from 2012 to 2018. Results illustrated remarkable seasonal isotopic variability, characterized by lower $\delta^{18}O$ and $\delta^{2}H$ values in June with an average of $-10‰$ and $-66.7‰$, respectively. Higher $\delta^{18}O$ and $\delta^{2}H$ values in July averaged $-6.7‰$ and $-39.5‰$, respectively. This clear isotopic variability is largely related to seasonal changes of moisture sources and hydrometeorological processes. These precipitation isotopic values were primarily determined by the amount of precipitation, relative humidity, and convective activity, but showed no correlation with air temperature. Backward trajectory model results showed that Xinjiang, northern China, the Arctic, central Asia, and the South China Sea (SCS) were the primary sources of precipitation for the study site with varying seasonal contributions. The maritime moisture source of the SCS primarily resulted in the lowest precipitation $\delta^{18}O$ values during the prevailing summer monsoon, which is mainly as a result of the strong convective activity and rainout processes along the air trajectory. The higher average deuterium excess (d-excess) value of precipitation in September indicated continental sources from central Asia (e.g., 75.4%) as land vapor recycling increases d-excess concentration in the atmosphere. These findings provide further insights into the main factors of precipitation isotopic variability related to atmospheric processes along the trajectory and the relevant factors in the monsoon regions.

SIGNIFICANCE STATEMENT: Recently, scientists and policy makers have become aware that Tibetan hydroclimate variability provides evidence of changes in regional and global circulation patterns that may result in the intensification of climate-driven extremes. However, these studies largely depend on crucial paleoclimate records of past precipitation isotopes in monsoon regions, which contain great uncertainties because of the complex relationship between climatic variability and precipitation isotopes. This study first presented a 7-yr isotopic dataset to understand the hydrological processes and climate dynamics controlling the isotopic variability in the northeastern Tibetan Plateau. The findings reveal important factors on the isotopic variability associated with atmospheric processes and their key climatic variables, which can enhance our interpretation of the paleoclimate records in monsoon regions.

1. Introduction

Stable isotopic signatures ($\delta^{18}O$ and $\delta^{2}H$) of paleo- and modern waters have provided novel insights into atmospheric processes, hydrological cycles, and paleoclimatic reconstruction (Gao et al. 2015; Shi et al. 2020a; Yao et al. 2013). Many studies in hydrology and paleoclimate fields greatly rely on the empirical relationships of precipitation isotopes based on

the amount of precipitation and temperature. In low-latitude and monsoon regions, a negative relationship between monthly precipitation $\delta^{18}O$ and the amount of precipitation is significant (the amount effect), whereas the well-known positive relationship between temperature and precipitation $\delta^{18}O$ is observed in high latitudes (Dansgaard 1964; Sánchez-Murillo et al. 2016). However, quantitatively identifying the potential factors controlling the variability of precipitation isotopes still remains highly uncertain, due to a series of complex hydrological processes such as upstream convection in the source regions, moisture sources, and rainout along transport trajectory (Tang et al. 2015; Wang et al. 2020; Zhou et al. 2019). Isotopes in precipitation are recorded as combined interactions of these factors, which makes them an important tool used to illustrate the precipitation formation's mechanism-induced processes including

dynamical and microphysical processes of atmospheric convection and paleoclimate change (Aggarwal et al. 2016; Dong et al. 2016; Ishizaki et al. 2012).

The Global Network of Isotopes in Precipitation (GNIP) launched by the International Atomic Energy Agency (IAEA) and the World Meteorological Organization (WMO) has provided valuable isotopic data to keep track of the hydrometeorological processes and moisture sources globally and regionally since 1961. However, the IAEA/WMO data coverage has been rated at certain times as being uneven based on the time and spatial scales. In addition, most of the IAEA/WMO monitoring sites have been terminated. The limited and discontinuous data from GNIP constrain our understanding of hydroclimatic variability, especially across the Tibetan Plateau (TP). To fill the data gap, systematic monitoring efforts for TP precipitation isotopes began in the1980s and include event-based and ice core data from the Tibetan Plateau Network of Isotopes for Precipitation (Gao et al. 2015; Tian et al. 2003; Yao et al. 2013). Recent studies using these data have made remarkable progress in identifying the dominant factors that define the precipitation isotope variability from the southern to northern TP, including the local precipitation amount effect (Tian et al. 2001; Yao et al. 2013; Zhang et al. 2019) and regional convective intensity (Rao et al. 2016; Wang et al. 2020). For example, Wang et al. (2020) found that the extent of cloud cover significantly determined the $\delta^{18}O$ in precipitation content at seasonal and interannual scales in southern TP. Zhang et al. (2019) showed that variations in precipitation isotopes are closely related with air mass transport and upstream convective processes along the trajectory in the central TP. Although these studies have helped elucidate the atmospheric processes that govern the precipitation isotopes variability in the TP, we must also have long-term high-resolution daily precipitation records of $\delta^{18}O$. This is essential to the understanding of local meteorological parameters, seasonality, and moisture sources for precipitation isotopes across the TP.

The high elevation and wide geographical coverage of TP act as a huge barrier to midlatitude westerlies and subsequently affect the global and regional atmospheric circulation. The westerlies' effect on the TP has led to many observations and modeling studies on the regional and local atmospheric processes determining the TP hydrological cycles (Gao et al. 2013; Yao et al. 2013). Many studies explain the atmospheric convection and regional water recycling using a combination of in situ measurement and Hybrid Single-Particle Lagrangian Integrated Trajectory (HYSPLIT) modeling of air parcel back trajectories on the TP to reveal the air mass movement and local moisture recycling processes (Bershaw et al. 2012; He et al. 2015). However, the relevant isotopic monitoring program is limited in the northeastern TP. Although previous isotopic studies conducted on the precipitation of the Qinghai Lake watershed were located in northeastern TP, limitations occurred during the short-term observation periods (Cui and Li 2015; Wu et al. 2019). For example, Cui and Li (2015) provided the first comprehensive analysis of variations in the isotopic composition of precipitation in the Qinghai Lake watershed and emphasized that the local lake evaporation vapor is an important moisture flux affecting the variations of precipitation isotopes. The authors established the local meteoric water line (LMWL) of
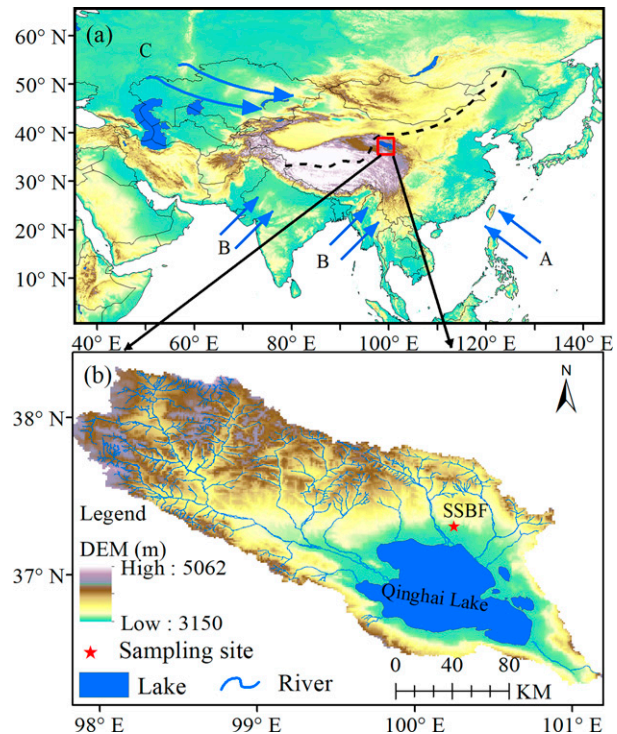

FIG. 1. (a) Geographical distribution of study area and (b) precipitation sampling site of Sanjiaocheng Sheep Breeding Farm (SSBF). Arrows with uppercase letters indicate the East Asian monsoon (A), Indian summer monsoon (B), and westerlies (C). The dashed line represents the modern Asian summer monsoon limit revised from Chen et al. (2016).

$\delta^2H = 7.86\ \delta^{18}O + 15.01$ on the monthly scale, which is different from the δ^2H–$\delta^{18}O$ correlation of $\delta^2H = 8.29(\pm 0.2)\ \delta^{18}O + 17.9(\pm 1.3)$ reported by Wu et al. (2019). In summary, these previous studies mainly focused on low-resolution isotopic data in the Qinghai Lake watershed, which constrained the potential mechanisms controlling the regional hydroclimate on a long-term scale.

To narrow the above knowledge gaps, we present a 7-yr-long daily precipitation isotopic dataset during the summer monsoon period from 2012 to 2018 at a Qinghai Lake site. Isotope ratios were analyzed in combination with local meteorological data and HYSPLIT air mass back trajectories to 1) characterize daily and seasonal variability of precipitation isotopes in northeastern TP, 2) explore the effects of local climate variables on isotopic variability, and 3) examine the control of moisture sources on seasonal variations of precipitation isotopes. Hence, this study supplemented the additional rainfall isotope time series on a daily scale to interpret the key drivers on the isotopic variability and paleoclimatic implications.

2. Materials and methods

a. Description of study area

The Qinghai Lake watershed (Fig. 1a with red box) is located at a climatic junction in northeastern TP where the

Asian summer monsoon (ASM) and the midlatitude westerlies interact frequently. The ASM can be divided into two subsystems: the Indian summer monsoon (ISM) and the East Asian summer monsoon (EASM) systems (An et al. 2012). The prevailing ASM carries more water vapor from the tropical Pacific and Indian Oceans, causing higher precipitation across northern China (Shi et al. 2020b; Yao et al. 2013). Dominated by the ASM and westerlies, this study area is climatically sensitive and ideally located for paleoclimatic studies (An et al. 2012; Thomas et al. 2016). The topography of the study area is complex with an elevation ranging from 3000 to 4500 m above mean sea level. Several basins, such as the Qinghai Lake Basin, the Gonghe Basin, and the Qaidam Basin, are distributed in northeastern TP and many are occupied by lakes. Climatic archives (e.g., lake sediments) in the region provide high-resolution and continuous climate proxies for environmental and climatic reconstructions (Chen et al. 2016; Henderson et al. 2010).

Qinghai Lake has a closed basin and no surface water outflow in northeastern TP. It is the largest inland saline lake in China. The lake is surrounded by several mountains, namely the Datong Mountain, Riyue Mountain, and South Qinghai Mountain. More than 40 rivers flow into Qinghai Lake, but most are intermittent. The annual precipitation in the Lake Qinghai catchment varies from 291 to 579 mm, with more than 70% falling in June through September; annual evaporation is larger than 1000 mm (Cai et al. 2015; Wu et al. 2015a). The annual average temperature ranges from $-1.1°$ to 4°C. The growing season at the study site is April through September. The monthly average precipitation amount and air temperature vary from 12.3 to 53.9 mm and from 1.1° to 6.2°C during the growing season, respectively (Fig. S1 in the online supplemental material).

b. Sample collection and isotopic analysis

A total of 326 event-based precipitation samples were collected at the field experimental site of the Sanjiaocheng Sheep Breeding Farm (SSBF; Fig. 1b; 37.26°N, 100.24°E, 3220 m), which is located on the north shore of Qinghai Lake. The sampling period covered the rainy season of June–September from 2012 to 2018. To avoid evaporation of samples, the liquid precipitation samples were collected immediately after the rainfall stopped and then filtered into 30-mL bottles with waterproof seals. All collected water samples were stored in a refrigerator at 4°C until the isotopic analysis was carried out. The daily surface air temperature and precipitation amount during the sampling periods were obtained from the weather station at the SSBF.

The δ^2H and $\delta^{18}O$ in precipitation were analyzed using a DLT-100 liquid water isotope analyzer (Los Gatos Research, Inc., Mountain View, CA) at the State Key Laboratory of Earth Surface Processes and Resource Ecology, Beijing Normal University, China. The measured isotopic values were expressed conventionally as δ values relative to V-SMOW (Vienna Standard Mean Ocean Water). The analytical precision of the precipitation sample was within $\pm1.0‰$ for δ^2H and $\pm0.3‰$ for $\delta^{18}O$.

Monthly average δ values were calculated from the event-based data weighted by the precipitation amount: $\bar{\delta} = \sum \delta_i P_i / \sum P_i$, where δ_i and P_i refer to isotopic compositions in daily precipitation and the corresponding precipitation amount, respectively.

c. HYSPLIT trajectory modeling and concentration weighted trajectory calculation

To explore possible moisture sources and transport paths, we conducted a back trajectory analysis using the HYSPLIT model version 4.0 (Sodemann et al. 2008; Stein et al. 2015). Back trajectory analysis was conducted for the 7-day (168 h) periods before arriving at the study site, considering that the residence time of global atmospheric water was approximately seven days during the rainy seasons (van der Ent and Tuinenburg 2017). The initial height was set at 1500 m above ground level (AGL) as the trajectory endpoint. Trajectories were calculated backward four times daily (at 0000, 0600, 1200, and 1800 UTC) in the HYSPLIT model throughout the 168 h. A cluster analysis tool in the HYSPLIT model was used to analyze multiple similar air mass trajectories, and merge them into the mean of clusters.

The concentration weighted trajectory (CWT) method using HYSPLIT simulation results was used to explore potential moisture sources and determine the precipitation isotopic variability (Bedaso and Wu 2020; Salamalikis et al. 2015). The CWT is calculated as

$$C_{ij} = \sum_{k=1}^{n} C_k \tau_{ijk} \Big/ \sum_{k=1}^{n} \tau_{ijk}, \tag{1}$$

where (i, j) are the indices of a grid cell, and C_{ij} is the weighted average concentration in a grid cell (i, j); k and n are the trajectory index and total number of precipitating trajectories, respectively. The term C_k is the concentration [deuterium excess (d-excess) and $\delta^{18}O$] measured on arrival of the trajectory k, and τ_{ijk} represents the residence time of the trajectory k in grid cell (i, j). The weighted values at each grid cell represent the composition that can be expected at the receptor site if an air parcel travels through the spatial grid.

d. Meteorological data and statistical analysis

To assess the convective intensity of precipitation, the National Oceanic and Atmospheric Administration (NOAA) interpolated outgoing longwave radiation (OLR) for 2012–18 with a spatial resolution of 2.5° × 2.5° are available at https://psl.noaa.gov/data/gridded/ (Su et al. 2000; Zhang et al. 2019). For HYSPLIT modeling, the HYSPLIT-compatible meteorological dataset was derived from the NCEP–NCAR Global Data Assimilation System (GDAS) reanalysis dataset with a spatial resolution of 1° × 1° including temperature (°C), specific humidity (g kg^{-1}), rainfall (mm h^{-1}), height (m AGL), and geographical coordinates for the air parcel (Draxler and Hess 1998; Stein et al. 2015).

A multivariate linear regression was used to identify the combined possible factors on the variations of isotopes in

TABLE 1. Statistics results of $\delta^{18}O$, δ^2H, and d-excess value in daily precipitation events across seasons. Ave$_w$, Min, Max, and SD represent the weighted-average value, minimum, maximum, and standard deviation of $\delta^{18}O$, δ^2H, and d-excess value, respectively.

| | $\delta^{18}O$ (‰) | | | | δ^2H (‰) | | | | d-excess (‰) | | | | |
	Ave$_w$	Min	Max	SD	Ave$_w$	Min	Max	SD	Ave$_w$	Min	Max	SD	N
June	−6.7	−13.6	2.1	3.5	−39.5	−94.5	33.4	27.6	14.1	−0.6	26.2	5.7	56
July	−10	−18.2	5.1	5.0	−66.7	−141.4	49.6	40.2	13.3	−2.2	22.4	4.8	79
August	−8.5	−17.3	4.3	4.5	−53.0	−122.9	47.0	37.2	15.1	−6.1	31.4	7.1	120
September	−7.9	−18.6	3.6	4.2	−44.0	−128.6	48.3	33.8	19.2	7.1	29.3	5.0	71
All	−8.6	−18.6	5.1	4.3	−54.9	−141.4	49.6	34.7	15.2	−6.1	31.4	5.7	326

precipitation. The multivariate regression model is expressed as follows:

$$\delta^{18}O = \beta_1 x_1 + \beta_2 x_2 + \cdots + \beta_n x_n + \beta_0, \qquad (2)$$

where β_n and x_n represent the partial regression coefficient and the potential independent variables such as air temperature, precipitation amount, relative humidity, and OLR; β_0 and n are the intercept and number of independent variables, respectively.

3. Results

a. Isotopic variations in precipitation

The stable isotopic compositions in precipitation collected at the Qinghai Lake site from 2012 to 2018 are summarized in Table 1 and Fig. 2. All original data are presented in Table S1 in the online supplemental material. During the entire observation period, daily data spread a large range in isotopic compositions of precipitation: precipitation $\delta^{18}O$ values varied from −18.6‰ to 4.3‰ with an amount-weighted average of −8.6‰; δ^2H ranged from −141.4‰ to 55.2‰ with an amount-weighted average of −53.8‰. Daily deuterium excess (d-excess = $\delta^2H - 8 \times \delta^{18}O$) values showed a large variability from −6.1‰ to 31.4‰, with an amount-weighted average of 15.2 ‰ (Fig. 2 and Table 1), which is greater than the global average d-excess of 10‰ (Dansgaard 1964).

The majority of precipitation events were collected in July and August (61%), and accounted for 64.9% of the total precipitation amount during the entire period. The seasonal variations of precipitation isotope data were remarkable from June to September. The daily δ^2H, $\delta^{18}O$, and d-excess data displayed a high degree of variability across seasons with the highest variability in July and the lowest in June (Table 1).
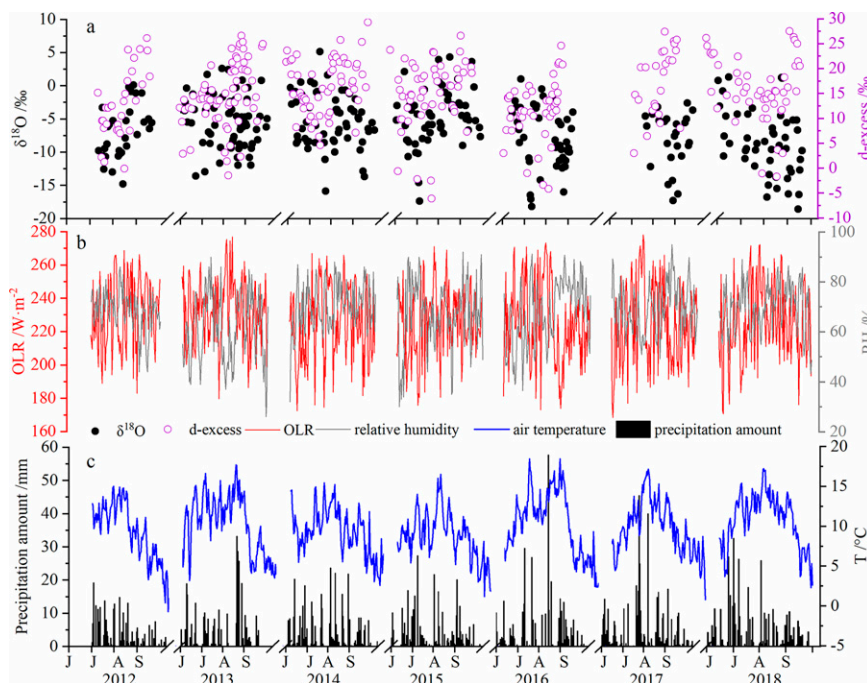

FIG. 2. Daily distributions of (a) precipitation isotopes ($\delta^{18}O$ and d-excess), (b) relative humidity (RH) and outgoing longwave radiation (OLR), and (c) precipitation amount (P) and air temperature (T) from 2012 to 2018.
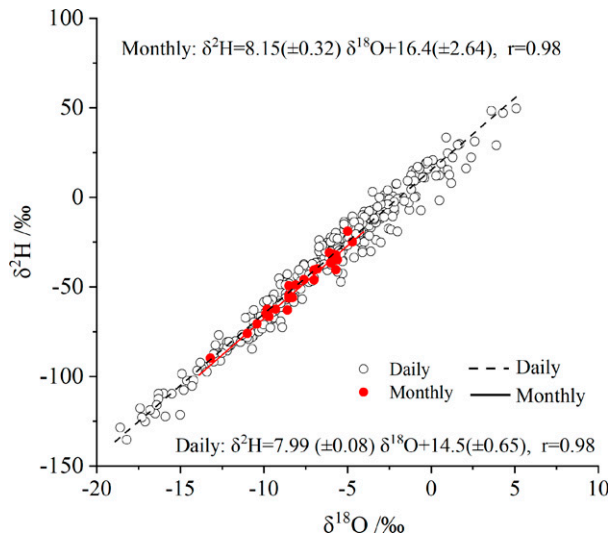
FIG. 3. Scatterplot between $\delta^{18}O$ and δ^2H in precipitation from the Qinghai Lake site on daily and monthly scales.

The lowest precipitation isotopic values (δ^2H, $\delta^{18}O$, and d-excess) were found in July ($-10‰$ and $-66.7‰$ for $\delta^{18}O_w$ and δ^2H_w, respectively). Conversely, the highest observed precipitation δ^2H and $\delta^{18}O$ values were in June ($-6.7‰$ for

$\delta^{18}O_w$ and $-39.5‰$ for δ^2H_w as shown in Fig. 2 and Table 1). The highest average d-excess value was observed in September (19.2‰) compared to other months, ranging from 13.3‰ to 15.1‰ (Table 1). The high $\delta^{18}O$ and δ^2H values in June are likely associated with moisture sources, which brings the enriched isotopic compositions of water vapor along the trajectory paths (Dansgaard 1964).

b. Local meteoric water lines

Figure 3 shows a robust linear regression relationship between δ^2H and $\delta^{18}O$ based on the daily and monthly precipitation events during summer monsoon periods in the Qinghai Lake watershed, defined as the LMWL. The slope and intercept of the δ^2H–$\delta^{18}O$ relationship on the daily scale [$\delta^2H = 7.99 (\pm0.08) \times \delta^{18}O + 14.5 (\pm0.65)$, $r = 0.98$] was slightly lower than that on the monthly scale [$\delta^2H = 8.15 (\pm0.32) \times \delta^{18}O + 14.8 (\pm2.64)$, $r = 0.98$] and annual scale [$\delta^2H = 8.7 (\pm0.6) \times \delta^{18}O + 21.4 (\pm5.1)$, $r = 0.99$]. Both daily and monthly slopes of LMWL were close to the global meteoric water line (GMWL: $\delta^2H = 8 \times \delta^{18}O + 10$) (Craig 1961).

To explore the seasonal influence on the LMWL, Fig. 4 indicates that the variations in the precipitation isotopes (δ^2H and $\delta^{18}O$) from July to September had a greater range than those in June. The LMWLs for all months had similar slopes, which was close to the slope of GMWL. The LMWL intercepts presented distinctly different values with the lowest in
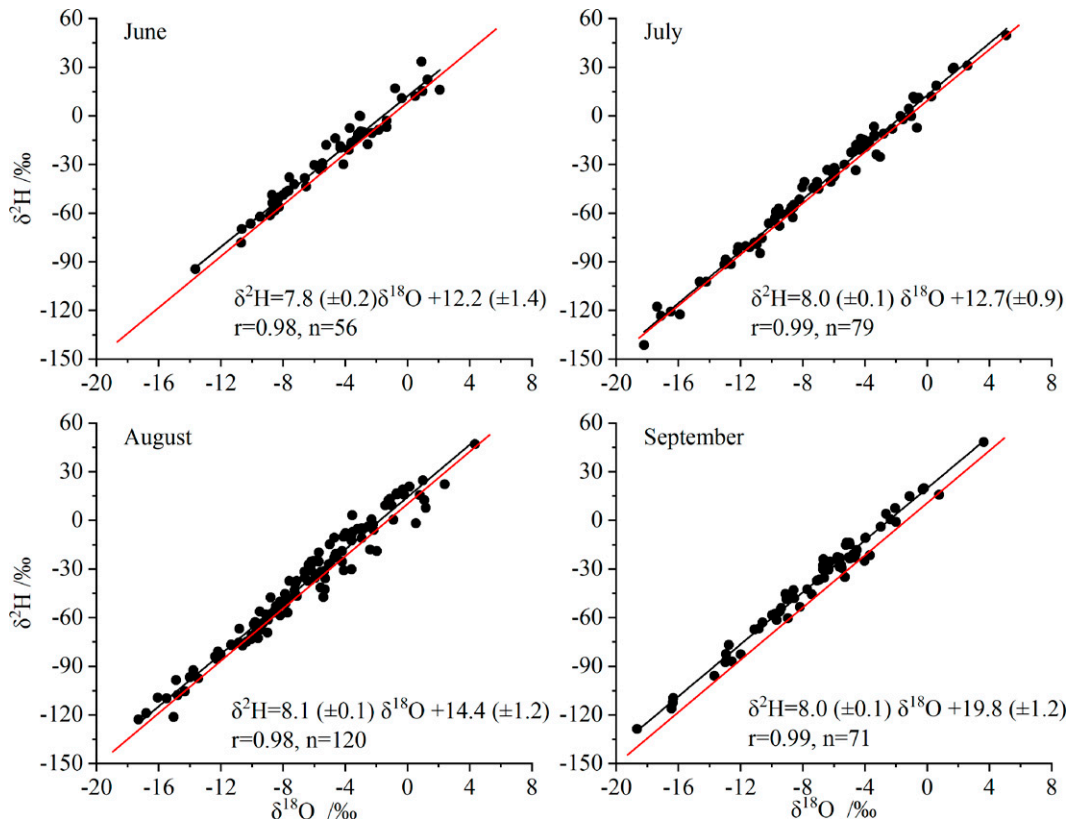

FIG. 4. Seasonal LMWLs for the Qinghai Lake site from June to September. The red line represents the GMWL ($\delta^2H = 8 \times \delta^{18}O + 10$).

TABLE 2. Comparison of the volume-weighted average isotopic compositions ($\delta^{18}O_w$, δ^2H_w, d-excess$_w$) and the Pearson's correlation coefficients (r) between $\delta^{18}O$ and amount of precipitation from 2012 to 2018. P and N represent the sum precipitation amount each year and the sampling number during the observation period, respectively. One asterisk (*) and two asterisks (**) represent $p < 0.01$ and $p < 0.05$, respectively.

Year	$\delta^{18}O$ & δ^2H			$\delta^{18}O_w$ (‰)	δ^2H_w (‰)	d-excess$_w$ (‰)	N	r	P (mm)
	a	b	r						
2012	8.7	18.0	0.98*	−8.9	−8.9	12.3	31	−0.52*	390.8
2013	7.8	13.9	0.98*	−7.8	−47.3	15.1	65	−0.48*	398.8
2014	8.1	16.3	0.99*	−7.4	−43.7	15.5	58	−0.39*	502.4
2015	7.8	14.8	0.98*	−7.2	−40.2	17.4	55	−0.41*	325.7
2016	7.8	9.6	0.99*	−11.5	−79.2	12.8	43	−0.68*	403.3
2017	8.0	17.2	0.98*	−8.9	−52.7	18.5	25	−0.44**	344.9
2018	7.9	15.3	0.98*	−9.6	−61.5	15.3	49	−0.58*	412.1

June (12.2‰), close to the GMWL, and the highest in September (19.8‰). These differences are associated with meteorological source conditions and local atmospheric conditions at the study site such as subcloud re-evaporation (Guan et al. 2013; Wu et al. 2015b). Similarly, the slopes of the LMWL were close to 8 during the observation period from 2013 to 2018 except in 2012 (Table 2).

c. Relationships between precipitation isotopes and climatic variables

The relationships between precipitation $\delta^{18}O$ values, d-excess, and local climatic variables (e.g., amount of precipitation, air temperature, and relative humidity) were analyzed to assess their local influence (Fig. 5, Table 3, and Table S3),
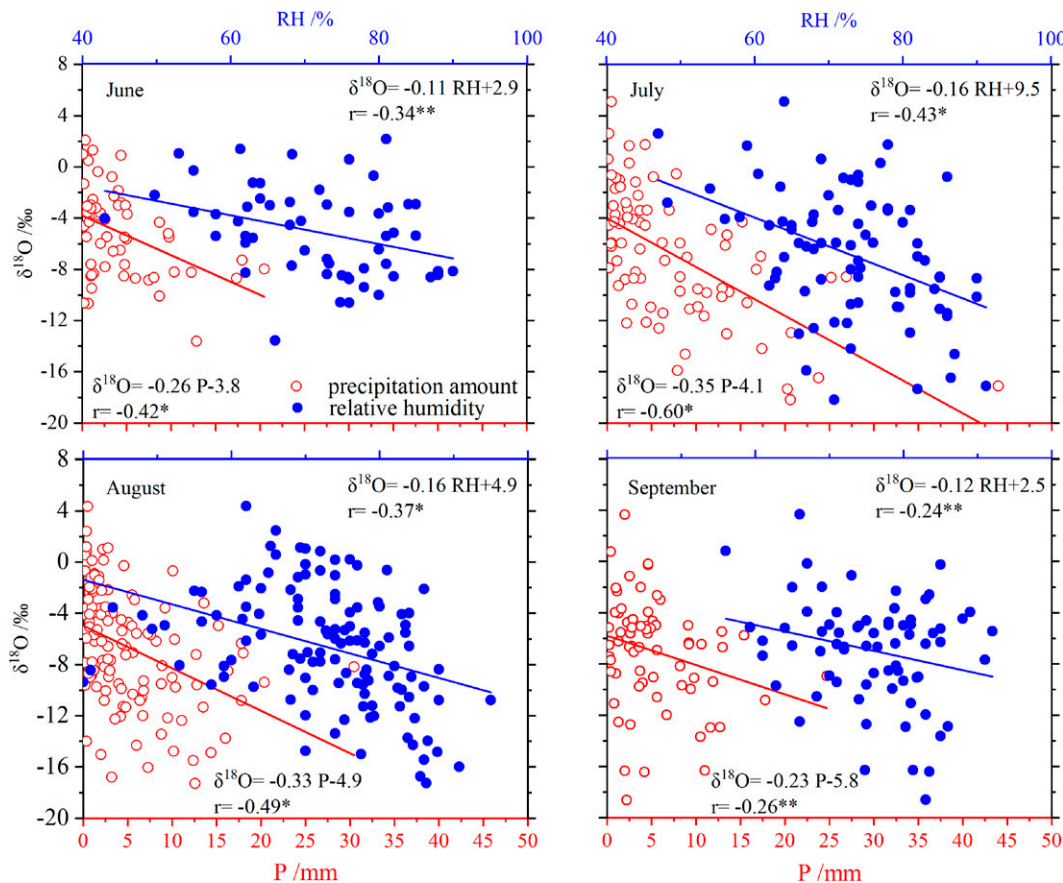

FIG. 5. Bivariate plots of precipitation $\delta^{18}O$ values, with precipitation amount (P) represented by red open circles and the relative humidity (RH) represented by blue solid circles, across seasons.

TABLE 3. Pearson's correlation of precipitation δ^{18}O and d-excess with climatic variables. r and p are Pearson's correlation coefficient and significance level, respectively.

Variables	Correlation with daily δ^{18}O		Correlation with daily d-excess		Correlation with monthly δ^{18}O		Correlation with monthly d-excess	
	r	p	r	p	r	p	r	p
Relative humidity	−0.36	0	0.13	0.02	−0.26	0.2	0.323	0.12
Air temperature	0.009	0.76	−0.44	0	−0.23	0.27	−0.38	0.06
Precipitation	−0.45	0	0.07	0.22	−0.42	0	−0.294	0.14
OLR	0.22	0	0.07	0.22	0.29	0.14	−0.22	0.9

which varied at the daily and monthly scales. Significant correlations ($p < 0.001$) of daily precipitation δ^{18}O values with precipitation amount (P), relative humidity (RH), and OLR were found, whereas no significant correlation was found between δ^{18}O and air temperature (T) (Table 3). Comparatively, no significant correlations were found when comparing precipitation δ^{18}O values with both RH and OLR at the monthly scale (Table 3). A significant negative relationship between daily d-excess and T was observed while a weak correlation with other climatic variables was observed (Table 3). However, monthly correlations between precipitation d-excess and climatic variables were not significant (Table 3). To explain the effects of seasonal climate variables on precipitation δ^{18}O, Fig. 5 shows the statistically significant negative correlations of precipitation δ^{18}O values with RH and P from June to September. Pearson's correlation coefficients varied from −0.24 (September) to −0.60 (July).

On the basis of the above linear correlation analysis, a multivariate regression model of daily precipitation δ^{18}O was created using stepwise regressions with combinations of four meteorological factors. This model with precipitation amount and relative humidity did a better job of predicting precipitation δ^{18}O than other models including OLR and T. The multivariate regression equation is as follows:

$$\delta^{18}O = 4.3 - 0.27P - 0.13RH(R^2 = 0.51, \ p < 0.01, \ n = 326). \tag{3}$$

The multivariate regression exhibited a significant Pearson's coefficient of determination (R^2) of 0.51 ($p < 0.01$), indicating that the coupled effects of RH and P accounted for 51% of the precipitation δ^{18}O variability at the study site.

4. Discussion

a. Impacts of local climate variables on precipitation isotopes

1) PRECIPITATION AMOUNT EFFECT

Precipitation isotopes integrate the combined effects of oceanic surface evaporation, rainout processes during moisture transport, local precipitation processes, and convective activity (Ansari et al. 2020; Dansgaard 1964; Risi et al. 2008). The potential factors controlling the precipitation isotopes were analyzed at different time scales according to available field data such as temperature, precipitation amount, relative humidity, and OLR in this study. The effect of monthly mean precipitation is often found in low-latitude regions (Risi et al. 2008; Vuille et al. 2005), which is not remarkable in midlatitude regions and never found in the polar regions. However, a significantly negative correlation of precipitation δ^{18}O with an amount of precipitation was found on the daily ($r = -0.45$) and monthly ($r = -0.42$) scales in the study site (Table 2), which indicates that the precipitation amount played a dominant role in the variations of isotopic composition in precipitation during summer monsoon periods at this site. The significant effect observed in the summer monsoon periods could probably be attributed to the increased convective activity controlling the isotopic composition in precipitation (Tharammal et al. 2017). That is because the stronger the convective nature of intensive precipitation events, the higher the total amount of precipitation and thus the more depleted the isotopic composition of precipitation. OLR is the total amount of thermal radiation emitted from Earth to interplanetary space, and is widely used to reflect convective activity (Ansari et al. 2020; Wang et al. 2020). A significant positive relationship between OLR and precipitation δ^{18}O was observed (Table 3), which indicated that the isotopic composition in precipitation was partly impacted by convective processes during summer monsoon periods. Dong et al. (2016) found that convective activity was more intense and frequent during the summer across the TP, resulting in intensive precipitating processes, thereby depleting the isotopic composition of water vapor and precipitation (Tian et al. 2020). Cui and Li (2015) also demonstrated that the remarkable convective activity in the regional water cycle of Qinghai Lake had a great influence on annual precipitation amount and isotopic compositions in precipitation during the summer seasons.

In this study, the amount effect was most dominant in July and August (Fig. 5). The average monthly δ^{18}O values in July and August were lowest with values of −10‰ and −8.5‰, respectively. This variation was primarily attributed to the fact that July and August are in the prevailing summer monsoon, when most of the water vapor stemmed from low-latitude marine regions (Cui and Li 2015; Zhang et al. 2019). The marine source regions feed a huge percentage of warm, humid moisture and produce strong convective activities with large amounts of precipitation during the prevailing summer monsoon periods (see section 4b). This resulted in the remarkable isotopic depletions in the study site and the enhanced precipitation effect in July and August. This effect is generally
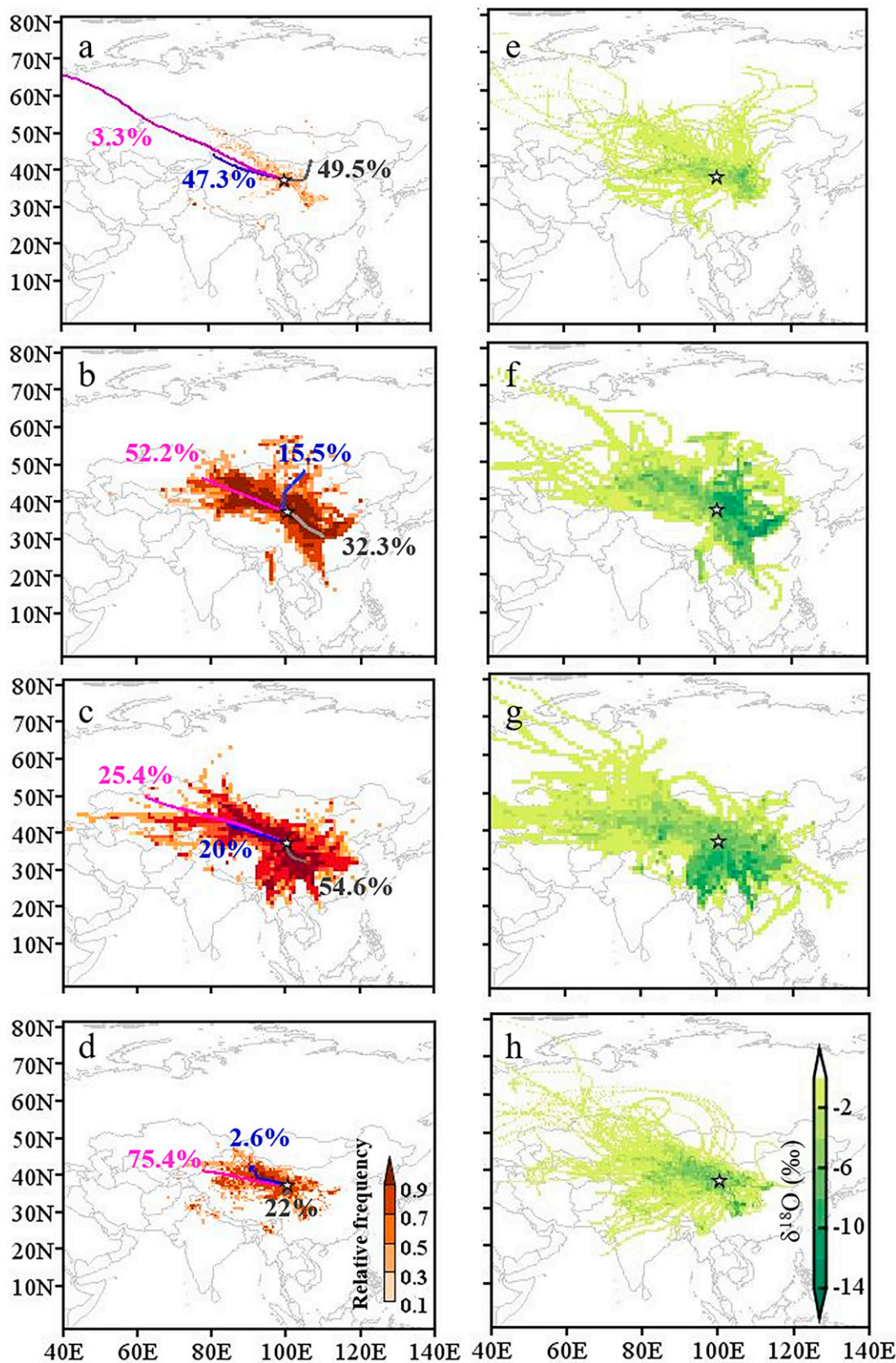
FIG. 6. (left) Trajectory frequency with color cluster lines and (right) concentration field of precipitation $\delta^{18}O$ in (a),(e) June, (b),(f) July, (c),(g) August, and (d),(h) September. Stars represent the study site.

TABLE 4. Statistics results of seasonal isotopic compositions of precipitation from different moisture sources.

	Sources	Trajectory frequency (%)	P (mm)	T (°C)	RH (%)	$\delta^{18}O_w$ (‰)	δ^2H_w (‰)	d-excess$_w$ (‰)
Jun	Xijiang Inland	47.3	95.1	8.9	68.1	−6.5	−36.6	15.5
	Northern China	49.5	145.0	8.7	74.4	−7.0	−42.1	13.8
	Arctic	3.3	4.2	5.8	73.1	−8.5	−47.8	20.6
Jul	Xijiang Inland	52.2	203.9	10.3	69.2	−8.2	−49.4	16.1
	Northern China	15.5	37.1	9.0	69.2	−4.1	−17.9	15.2
	South China Sea	32.3	348.9	11.2	77.4	−11.6	−82.0	10.9
Aug	Central Asia	25.4	97.8	9.0	65.6	−5.6	−28.6	15.8
	Xijiang Inland	20	115.1	10.6	71.8	−6.9	−41.2	13.8
	South China Sea	54.6	391.5	10.7	76.7	−9.7	−62.6	15.2
Sep	Central Asia	75.4	295.0	5.6	70.7	−7.7	−40.7	20.7
	Xijiang Inland	22	38.5	5.6	75.9	−7.3	−39.9	18.8
	South China Sea	2.6	40.9	6.3	79.4	−8.1	−49.2	15.2
Jun–Sep	South China Sea	47.8	1139.9	9.9	77.1	−9.7	−63.2	14.4
	Xijiang Inland	47.6	615.1	8.3	70.4	−6.9	−39.2	16.6
	Central Asia	4.6	53.3	9.3	62.9	−5.2	−25.3	16.2

observed in tropical and monsoon climatic regions, characterized by depleted isotopic values (Wu et al. 2015b; Xie et al. 2011). Interannually, however, correlations between the weighted annual average $\delta^{18}O$ values and annual precipitation amounts were not significant ($r = -0.29$, $p > 0.05$) during the period between 2012 and 2018. Moreover, what controls the interannual variability of precipitation isotopes is relatively complex during the monsoon periods and needs to be further explored in the future when long-term datasets can be available. These results on isotopic composition at different time scales were similar in regions such as the southeastern TP (Shi et al. 2020a; Yu et al. 2017) and the subtropical monsoon regions of Changsha and Guangzhou (Xie et al. 2011; Zhou et al. 2019).

2) EFFECTS OF TEMPERATURE AND OTHER ENVIRONMENTAL CONDITIONS

In the study, there was no significant relationship between $\delta^{18}O$ values and surface air temperature (Table 3), indicating that temperature was not the main factor affecting isotopic composition in precipitation. A weak negative correlation between $\delta^{18}O$ and RH was observed throughout the entire period (Table 3), indicating that the isotopic composition of precipitation experienced some degree of evaporation fractionation during the falling processes (Peng et al. 2005; Salamalikis et al. 2016). Low relative humidity at the sampling site could potentially promote subcloud evaporation and further produce enriched precipitation $\delta^{18}O$ in the remaining rains (Aemisegger et al. 2015). In our study, small precipitation events ($P < 5$ mm) that accounted for 62.5% of the total precipitation events presented the most enriched average $\delta^{18}O$ value of −5.7 ‰ during the sampling periods (Table S2). This category of small precipitation events (lower falling velocities) was characterized by lower relative humidity, which promoted the enrichment of isotopic compositions in small precipitation events.

Based on the aforementioned correlation analysis, precipitation $\delta^{18}O$ had a higher Pearson's correlation coefficient with amount of precipitation than with RH and OLR at both daily and monthly time scales. The variability in precipitation isotopes was coupled with multiple meteorological factors such as RH and P (Le Duy et al. 2018). Both precipitation amount and relative humidity were thus used in the multivariate analysis to explain the isotopic variability. The regression result in Eq. (3) indicated that the combined precipitation amount and RH explained 51% of the precipitation isotopic variability.

b. Effects of moisture sources on precipitation isotopes

The present study site is situated in a critical transitional zone where the East Asian monsoon, Indian summer monsoon, and westerly circulation meet (Fig. 1), resulting in complex moisture sources and precipitation patterns (An et al. 2012). Figure 6 tracks the isotopic compositions of air mass trajectories passing through a region. According to the cluster analysis of the HYSPLIT trajectory model, the main moisture sources identified were from the inland area of the Xinjiang Uygur Autonomous Region (hereinafter Xinjiang Inland), northern China, the Arctic, central Asia, and the South China Sea (SCS) (Fig. 6 and Table 4). However, the relative contribution of moisture sources varied between months (Fig. 6). In June, the continental moisture source from northern China (49.5%) and Xinjiang Inland (49.5%) were dominant whereas the maritime moisture source from SCS became dominant during the prevailing monsoon periods. The contributing proportion of the SCS increased from 32.3% in July to 54.6% in August. The overall average $\delta^{18}O$ value was the lowest for the SCS source (−11.6‰) and the highest for continental sources from northern China (−4.1‰; Table 4), which largely determined the precipitation isotopes at the Qinghai Lake site.

The sources of precipitating trajectories exhibited remarkable seasonal variations, showing the lowest $\delta^{18}O$ values in July and the highest $\delta^{18}O$ values in June (Figs. 6e–h and
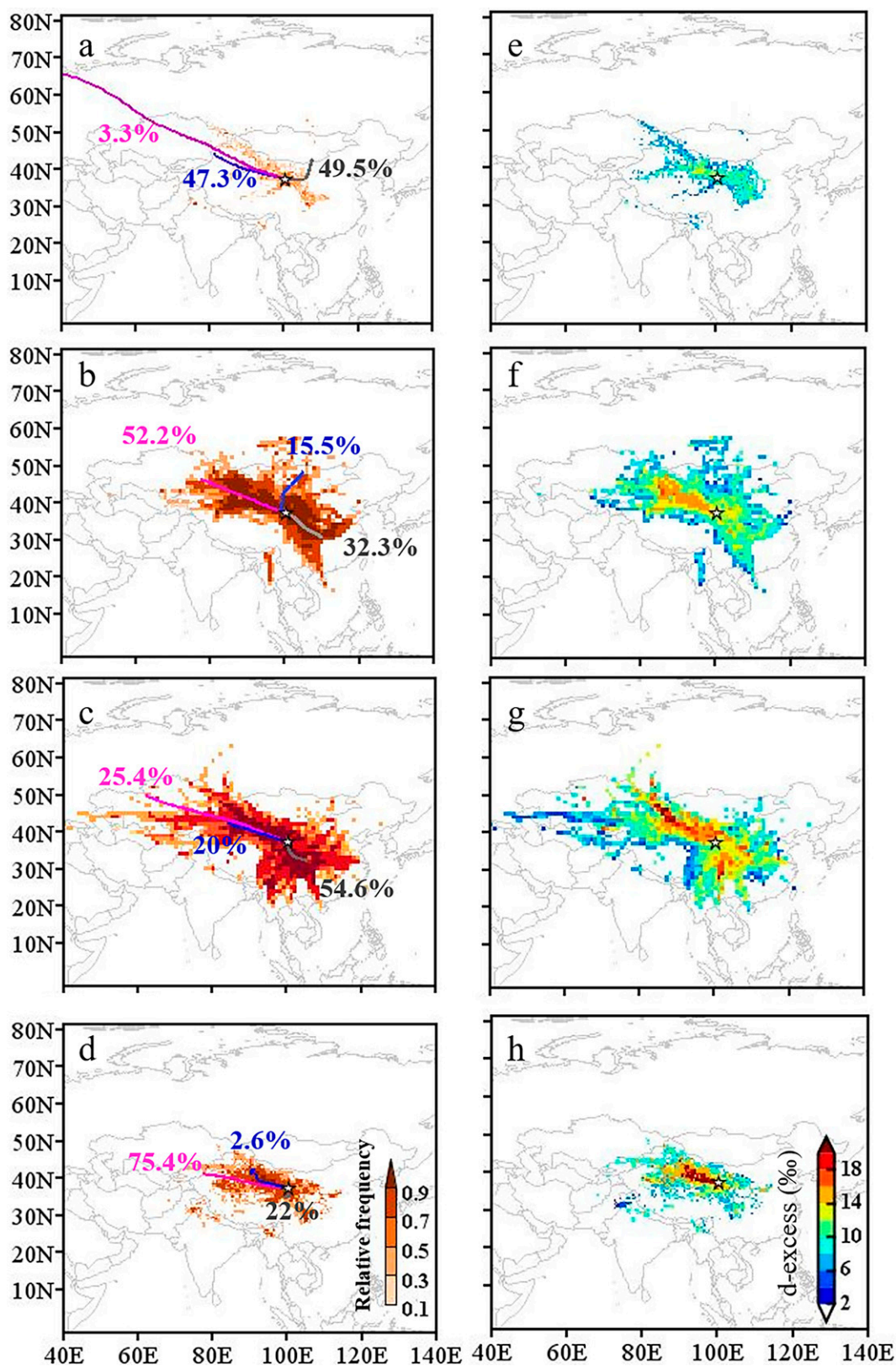
FIG. 7. (left) Trajectory frequency with color cluster lines and (right) concentration field of precipitation d-excess in (a),(e) June, (b),(f) July, (c),(g) August, and (d),(h) September. Stars represent the study site.

Table 4). The average $\delta^{18}O$ values of the Xinjiang Inland source ranged from $-8.2‰$ to $-6.5‰$ during June to September, whereas other continental source from central Asia and northern Asia had relatively higher $\delta^{18}O$ values from $-7.7‰$ to $-4.1‰$ (Table 4). According to the isotopic evaporation modeling, the isotopes of atmospheric water vapor at the study site are affected by the evaporated water vapor from surface waters (Craig and Gordon 1965). Hence, the enriched precipitation $\delta^{18}O$ values in June could be derived from the evaporation of soil water (Kurita and Yamada 2008) and $\delta^{18}O$-enriched surface waters in the semiarid and arid regions (Burnik Šturm et al. 2017; Chen et al. 2018; Hao et al. 2019). On the other hand, the gradual increase of the depleted moisture from the maritime source of SCS in July ($-11.6‰$) and August ($-9.7‰$) could result from strong convective activities and rainout processes along the air trajectory, and the impacts of extreme weather (e.g., tropical cyclones) or the remnants of these extreme weather events that affect the study region. Previous studies demonstrated that tropical cyclones or typhoons produce more depleted precipitation $\delta^{18}O$ values than other summer precipitation events (Gedzelman and Lawrence 1990; Wu et al. 2015b; Xu et al. 2019). For example, the remnants of Typhoon Haima affected the monsoon regions of China, resulting in lower precipitation $\delta^{18}O$ values (Huang et al. 2019).

Precipitation d-excess values also exhibited seasonal variations, characterized by higher values in September (19.2‰) and lower values in July (13.3‰) (Fig. 2 and Table 1). The seasonal variations of precipitation d-excess values were closely associated with variations of relative humidity in the source regions (Benetti et al. 2014) and further alterations along the air trajectory (Guan et al. 2013). Figure 7 shows the spatial distributions of air mass trajectory frequency and the d-excess concentration across different seasons. The precipitation d-excess values in June show lower spatial heterogeneity across various moisture regions whereas the higher spatial variability of the d-excess value is found from July to September (Figs. 7e–h). This seasonal variation of d-excess may indicate that atmospheric moisture included high variability of the d-excess values or complex atmospheric conditions from July to September. Precipitation d-excess values can be altered as the air mass transports toward the study site. For instance, average d-excess value was higher in September in precipitation derived from continental sources of central Asia (e.g., 75.4%) as land vapor recycling enhances d-excess concentration in the atmosphere (d-excess $> 20‰$; Table 4). Figure 7 also shows that the lower d-excess values of air trajectories from the SCS varied from 10.9‰ in July to 15.2‰ in August and September with relatively higher trajectory frequency, corresponding to the higher relative humidity shown in Table 4. Therefore, the low d-excess values are closely related to moisture sources from the low-latitude oceanic regions, because of less kinetic isotopic fractionation under the humid conditions (Benetti et al. 2014; Tian et al. 2020).

5. Conclusions

A 7-yr daily observation of stable isotopes in precipitation was launched during the summer monsoon seasons from 2012 to 2018 at the Qinghai Lake site in northwestern TP to explore the variations of precipitation isotopes and the dominant controlling factors regarding hydrometeorological processes and moisture sources. Key findings are summarized as follows:

1) Precipitation δ^2H and $\delta^{18}O$ values presented remarkable seasonal variations, indicating changes in precipitation isotopes in response to seasonal variations of moisture sources and hydrometeorological conditions.
2) On a seasonal scale, the amount effect of precipitation was a key factor determining the isotopic compositions in precipitation during the prevailing summer monsoon season in July and August; thus, the July and August precipitation was closely associated with enhanced convective activity.
3) The present study site received various proportions of moisture from multiple sources during the summer monsoon periods. In June, the continental moisture source from northern China and Xinjiang Inland was dominant whereas the maritime moisture source of the SCS gradually played a dominant role in the moisture contribution during the prevailing monsoon period.
4) The precipitation isotopic compositions of $\delta^{18}O$ and d-excess values exhibited remarkable seasonal variability, which is associated with moisture sources largely controlled the isotopic compositions of precipitation at the sampling site.

Overall, these findings advance our understanding of the temporal variations of precipitation stable isotopes in a Qinghai Lake site of the northwestern TP and shed new light on the study of climatic and environmental controls based on precipitation stable isotope composition in monsoon regions.

REFERENCES

Aemisegger, F., and Coauthors, 2015: Isotope meteorology of cold front passages: A case study combining observations and modeling. *Geophys. Res. Lett.*, **42**, 5652–5660, https://doi.org/10.1002/2015GL063988.

Aggarwal, P. K., and Coauthors, 2016: Proportions of convective and stratiform precipitation revealed in water isotope ratios. *Nat. Geosci.*, **9**, 624–629, https://doi.org/10.1038/ngeo2739.

An, Z., and Coauthors, 2012: Interplay between the westerlies and Asian monsoon recorded in Lake Qinghai sediments since 32 ka. *Sci. Rep.*, **2**, 619, https://doi.org/10.1038/srep00619.

Ansari, M. A., J. Noble, A. Deodhar, and U. Saravana Kumar, 2020: Atmospheric factors controlling the stable isotopes ($\delta^{18}O$ and δ^2H) of the Indian summer monsoon precipitation

in a drying region of eastern India. *J. Hydrol.*, **584**, 124636, https://doi.org/10.1016/j.jhydrol.2020.124636.

Bedaso, Z., and S.-Y. Wu, 2020: Daily precipitation isotope variation in Midwestern United States: Implication for hydroclimate and moisture source. *Sci. Total Environ.*, **713**, 136631, https://doi.org/10.1016/j.scitotenv.2020.136631.

Benetti, M., and Coauthors, 2014: Deuterium excess in marine water vapor: Dependency on relative humidity and surface wind speed during evaporation. *J. Geophys. Res. Atmos.*, **119**, 584–593, https://doi.org/10.1002/2013JD020535.

Bershaw, J., S. M. Penny, and C. N. Garzione, 2012: Stable isotopes of modern water across the Himalaya and eastern Tibetan Plateau: Implications for estimates of paleoelevation and paleoclimate. *J. Geophys. Res.*, **117**, D02110, https://doi.org/10.1029/2011JD016132.

Burnik Šturm, M., O. Ganbaatar, C. C. Voigt, and P. Kaczensky, 2017: First field-based observations of δ^2H and $\delta^{18}O$ values of event-based precipitation, rivers and other water bodies in the Dzungarian Gobi, SW Mongolia. *Isotopes Environ. Health Stud.*, **53**, 157–171, https://doi.org/10.1080/10256016.2016.1231184.

Cai, Y., and Coauthors, 2015: Variability of stalagmite-inferred Indian monsoon precipitation over the past 252,000 y. *Proc. Natl. Acad. Sci. USA*, **112**, 2954–2959, https://doi.org/10.1073/pnas.1424035112.

Chen, F., and Coauthors, 2016: Holocene moisture and East Asian summer monsoon evolution in the northeastern Tibetan Plateau recorded by Lake Qinghai and its environs: A review of conflicting proxies. *Quat. Sci. Rev.*, **154**, 111–129, https://doi.org/10.1016/j.quascirev.2016.10.021.

Chen, H., and Coauthors, 2018: Identifying evaporation fractionation and streamflow components based on stable isotopes in the Kaidu River Basin with mountain–oasis system in northwest China. *Hydrol. Processes*, **32**, 2423–2434, https://doi.org/10.1002/hyp.13176.

Craig, H., 1961: Isotope variations in meteoric waters. *Science*, **133**, 1702–1703, https://doi.org/10.1126/science.133.3465.1702.

——, and L. I. Gordon, 1965. Deuterium and oxygen 18 variations in the ocean and the marine atmosphere. *Marine Geochemistry*, D. R. Schink and J. T. Corless, Eds., University of Rhode Island, 277–374.

Cui, B.-L., and X.-Y. Li, 2015: Stable isotopes reveal sources of precipitation in the Qinghai Lake Basin of the northeastern Tibetan Plateau. *Sci. Total Environ.*, **527**, 26–37, https://doi.org/10.1016/j.scitotenv.2015.04.105.

Dansgaard, W., 1964: Stable isotopes in precipitation. *Tellus*, **16**, 436–468, https://doi.org/10.3402/tellusa.v16i4.8993.

Dong, W., and Coauthors, 2016: Summer rainfall over the southwestern Tibetan Plateau controlled by deep convection over the Indian subcontinent. *Nat. Commun.*, **7**, 10925, https://doi.org/10.1038/ncomms10925.

Draxler, R. R., and G. Hess, 1998: An overview of the HYSPLIT_4 modelling system for trajectories, dispersion, and deposition. *Aust. Meteor. Mag.*, **47**, 295–308, https://www.arl.noaa.gov/documents/reports/MetMag.pdf.

Gao, J., V. Masson-Delmotte, C. Risi, Y. He, and T. Yao, 2013: What controls precipitation $\delta^{18}O$ in the southern Tibetan Plateau at seasonal and intra-seasonal scales? A case study at Lhasa and Nyalam. *Tellus*, **65B**, 21043, https://doi.org/10.3402/tellusb.v65i0.21043.

——, and Coauthors, 2015: Reconstruction of precipitation $\delta^{18}O$ over the Tibetan Plateau since 1910. *J. Geophys. Res. Atmos.*, **120**, 4878–4888, https://doi.org/10.1002/2015JD023233.

Gedzelman, S. D., and J. R. Lawrence, 1990: The isotopic composition of precipitation from two extratropical cyclones. *Mon. Wea. Rev.*, **118**, 495–509, https://doi.org/10.1175/1520-0493(1990)118<0495:TICOPF>2.0.CO;2.

Guan, H., X. Zhang, G. Skrzypek, Z. Sun, and X. Xu, 2013: Deuterium excess variations of rainfall events in a coastal area of South Australia and its relationship with synoptic weather systems and atmospheric moisture sources. *J. Geophys. Res. Atmos.*, **118**, 1123–1138, https://doi.org/10.1002/jgrd.50137.

Hao, S., and Coauthors, 2019: Stable isotope evidence for identifying the recharge mechanisms of precipitation, surface water, and groundwater in the Ebinur Lake basin. *Sci. Total Environ.*, **657**, 1041–1050, https://doi.org/10.1016/j.scitotenv.2018.12.102.

He, Y., and Coauthors, 2015. Impact of atmospheric convection on south Tibet summer precipitation isotopologue composition using a combination of in situ measurements, satellite data, and atmospheric general circulation modeling. *J. Geophys. Res. Atmos.*, **120**, 3852–3871, https://doi.org/10.1002/2014JD022180.

Henderson, A. C., J. A. Holmes, and M. J. Leng, 2010: Late Holocene isotope hydrology of Lake Qinghai, NE Tibetan Plateau: Effective moisture variability and atmospheric circulation changes. *Quat. Sci. Rev.*, **29**, 2215–2223, https://doi.org/10.1016/j.quascirev.2010.05.019.

Huang, Y., and Coauthors, 2019: Precipitation isotopes formed by Typhoon Haimain in the Dongting Lake Basin. *Sci. Geogr. Sin.*, **39**, 1184–1190, https://doi.org/10.13249/j.cnki.sgs.2019.07.017.

Ishizaki, Y., and Coauthors, 2012: Interannual variability of $H_2^{18}O$ in precipitation over the Asian monsoon region. *J. Geophys. Res.*, **117**, D16308, https://doi.org/10.1029/2011JD015890.

Kurita, N., and H. Yamada, 2008: The role of local moisture recycling evaluated using stable isotope data from over the middle of the Tibetan Plateau during the monsoon season. *J. Hydrometeor.*, **9**, 760–775, https://doi.org/10.1175/2007JHM945.1.

Le Duy, N., I. Heidbüchel, H. Meyer, B. Merz, and H. Apel, 2018: What controls the stable isotope composition of precipitation in the Mekong Delta? A model-based statistical approach. *Hydrol. Earth Syst. Sci.*, **22**, 1239–1262, https://doi.org/10.5194/hess-22-1239-2018.

Peng, H., B. Mayer, A.-L. Norman, and H. R. Krouse, 2005: Modelling of hydrogen and oxygen isotope compositions for local precipitation. *Tellus*, **57B**, 273–282, https://doi.org/10.3402/tellusb.v57i4.16545.

Rao, P. S. P., and Coauthors, 2016: Sources of chemical species in rainwater during monsoon and non-monsoonal periods over two mega cities in India and dominant source region of secondary aerosols. *Atmos. Environ.*, **146**, 90–99, https://doi.org/10.1016/j.atmosenv.2016.06.069.

Risi, C., S. Bony, and F. Vimeux, 2008: Influence of convective processes on the isotopic composition ($\delta^{18}O$ and δD) of precipitation and water vapor in the tropics: 2. Physical interpretation of the amount effect. *J. Geophys. Res.*, **113**, D19306, https://doi.org/10.1029/2008JD009943.

Salamalikis, V., A. A. Argiriou, and E. Dotsika, 2015: Stable isotopic composition of atmospheric water vapor in Patras, Greece: A concentration weighted trajectory approach. *Atmos. Res.*, **152**, 93–104, https://doi.org/10.1016/j.atmosres.2014.02.021.

——, ——, and ——, 2016: Isotopic modeling of the sub-cloud evaporation effect in precipitation. *Sci. Total Environ.*, **544**, 1059–1072, https://doi.org/10.1016/j.scitotenv.2015.11.072.

Sánchez-Murillo, R., and Coauthors, 2016: Key drivers controlling stable isotope variations in daily precipitation of Costa Rica: Caribbean Sea versus eastern Pacific Ocean moisture sources. *Quat. Sci. Rev.*, **131**, 250–261, https://doi.org/10.1016/j.quascirev.2015.08.028.

Shi, X., and Coauthors, 2020a: Variability of isotope composition of precipitation in the southeastern Tibetan Plateau from the synoptic to seasonal time scale. *J. Geophys. Res. Atmos.*, **125**, e2019JD031751, https://doi.org/10.1029/2019JD031751.

Shi, Y., Z. Jiang, Z. Liu, and L. Li, 2020b: A Lagrangian analysis of water vapor sources and pathways for precipitation in East China in different stages of the East Asian summer monsoon. *J. Climate*, **33**, 977–992, https://doi.org/10.1175/JCLI-D-19-0089.1.

Sodemann, H., C. Schwierz, and H. Wernli, 2008: Interannual variability of Greenland winter precipitation sources: Lagrangian moisture diagnostic and North Atlantic Oscillation influence. *J. Geophys. Res.*, **113**, D03107, https://doi.org/10.1029/2007JD008503.

Stein, A. F., and Coauthors, 2015: NOAA's HYSPLIT atmospheric transport and dispersion modeling system. *Bull. Amer. Meteor. Soc.*, **96**, 2059–2077, https://doi.org/10.1175/BAMS-D-14-00110.1.

Su, W., J. Mao, F. Ji, and Y. Qin, 2000: Outgoing longwave radiation and cloud radiative forcing of the Tibetan Plateau. *J. Geophys. Res.*, **105**, 14 863–14 872, https://doi.org/10.1029/2000JD900201.

Tang, Y., and Coauthors, 2015: Effects of changes in moisture source and the upstream rainout on stable isotopes in summer precipitation—A case study in Nanjing, East China. *Hydrol. Earth Syst. Sci. Discuss.*, **12**, 3919–3944, https://doi.org/10.5194/hessd-12-3919-2015.

Tharammal, T., G. Bala, and D. Noone, 2017: Impact of deep convection on the isotopic amount effect in tropical precipitation. *J. Geophys. Res. Atmos.*, **122**, 1505–1523, https://doi.org/10.1002/2016JD025555.

Thomas, E. K., and Coauthors, 2016: Changes in dominant moisture sources and the consequences for hydroclimate on the northeastern Tibetan Plateau during the past 32 kyr. *Quat. Sci. Rev.*, **131**, 157–167, https://doi.org/10.1016/j.quascirev.2015.11.003.

Tian, L., V. Masson-Delmotte, M. Stievenard, T. Yao, and J. Jouzel, 2001: Tibetan Plateau summer monsoon northward extent revealed by measurements of water stable isotopes. *J. Geophys. Res.*, **106**, 28 081–28 088, https://doi.org/10.1029/2001JD900186.

——, and Coauthors, 2003: Oxygen-18 concentrations in recent precipitation and ice cores on the Tibetan Plateau. *J. Geophys. Res.*, **108**, 4293, https://doi.org/10.1029/2002JD002173.

——, and Coauthors, 2020: Control of seasonal water vapor isotope variations at Lhasa, southern Tibetan Plateau. *J. Hydrol.*, **580**, 124237, https://doi.org/10.1016/j.jhydrol.2019.124237.

van der Ent, R. J., and O. A. Tuinenburg, 2017: The residence time of water in the atmosphere revisited. *Hydrol. Earth Syst. Sci.*, **21**, 779–790, https://doi.org/10.5194/hess-21-779-2017.

Vuille, M., M. Werner, R. S. Bradley, and F. Keimig, 2005: Stable isotopes in precipitation in the Asian monsoon region. *J. Geophys. Res.*, **110**, D23108, https://doi.org/10.1029/2005JD006022.

Wang, D., and Coauthors, 2020: Indian monsoon precipitation isotopes linked with high level cloud cover at local and regional scales. *Earth Planet. Sci. Lett.*, **529**, 115837, https://doi.org/10.1016/j.epsl.2019.115837.

Wu, H., and Coauthors, 2015a: Evaporative enrichment of stable isotopes (δ^{18}O and δD) in lake water and the relation to lake-level change of Lake Qinghai, northeast Tibetan Plateau of China. *J. Arid Land*, **7**, 623–635, https://doi.org/10.1007/s40333-015-0048-6.

——, X. Zhang, L. Xiaoyan, G. Li, and Y. Huang, 2015b: Seasonal variations of deuterium and oxygen-18 isotopes and their response to moisture source for precipitation events in the subtropical monsoon region. *Hydrol. Processes*, **29**, 90–102, https://doi.org/10.1002/hyp.10132.

——, and Coauthors, 2019: Stable isotopes of atmospheric water vapor and precipitation in the northeast Qinghai-Tibetan Plateau. *Hydrol. Processes*, **33**, 2997–3009, https://doi.org/10.1002/hyp.13541.

Xie, L., G. Wei, W. Deng, and X. Zhao, 2011: Daily δ^{18}O and δD of precipitations from 2007 to 2009 in Guangzhou, South China: Implications for changes of moisture sources. *J. Hydrol.*, **400**, 477–489, https://doi.org/10.1016/j.jhydrol.2011.02.002.

Xu, T., and Coauthors, 2019: Stable isotope ratios of typhoon rains in Fuzhou, Southeast China, during 2013–2017. *J. Hydrol.*, **570**, 445–453, https://doi.org/10.1016/j.jhydrol.2019.01.017.

Yao, T., and Coauthors, 2013: A review of climatic controls on δ^{18}O in precipitation over the Tibetan Plateau: Observations and simulations. *Rev. Geophys.*, **51**, 525–548, https://doi.org/10.1002/rog.20023.

Yu, W., and Coauthors, 2017: Precipitation stable isotope records from the northern Hengduan Mountains in China capture signals of the winter India–Burma trough and the Indian summer monsoon. *Earth Planet. Sci. Lett.*, **477** (Suppl. C), 123–133, https://doi.org/10.1016/j.epsl.2017.08.018.

Zhang, T., and Coauthors, 2019: Controls of stable isotopes in precipitation on the central Tibetan Plateau: A seasonal perspective. *Quat. Int.*, **513**, 66–79, https://doi.org/10.1016/j.quaint.2019.03.031.

Zhou, H., and Coauthors, 2019: Variation of δ^{18}O in precipitation and its response to upstream atmospheric convection and rainout: A case study of Changsha station, south-central China. *Sci. Total Environ.*, **659**, 1199–1208, https://doi.org/10.1016/j.scitotenv.2018.12.396.